Using source maps for scheduling and data analysis: approaches and strategies

L. Petrov
NVI, Inc./NASA GSFC, Code 698, Greenbelt, 20771 MD, USA

Abstract. Since almost all the sources observed with VLBI at intercontinental baselines are resolved, information about source structure should be utilized during scheduling and analysis of geodetic VLBI experiments. I collected the database of images of ~ 4000 sources from analysis of VLBA and Australian LBA array observations. Analysis of images and calibrated visibilities allowed us to select a list of 230 of the best sources for including in geodetic observing schedules. These sources have a) a significant correlated flux density at long baselines, b) a significant compactness index, and c) a least asymmetric core. For these sources the coherence function depends mainly on the length of the projected baseline, and neglecting its dependence on baseline orientation produces errors in the coherence amplitude prediction less than 20%. Usage of source maps in the form of an expansion over a set of δ-functions in data reduction process requires great care. I found that the traditional hybrid CLEAN algorithm produces maps which are not always suitable for reduction of geodetic experiments, since the noise in data makes computation of the contribution of source structure to group delay highly instable.

Keywords. astrometry, data analysis, VLBI

1 Introduction

Almost all the sources observed with VLBI at intercontinental baselines are resolved and cannot be considered as point-like. The presence of detectable source structure affects both prediction of the amplitude of the coherence function and the observed value of group delay.

According to the van Cittert–Zernike theorem, the interferometric coherence function V is related to the source position vector $\vec{s}$, baseline vector $\vec{b}$, the angular frequency of radiation ω through the two-dimensional Fourier-transform of the source brightness distribution $I(\vec{p})$:

$$\begin{aligned} \mathcal{F}(\vec{b},\omega) \quad &= \int\int I(\vec{p},\omega) e^{-i\frac{\omega}{c}\vec{b}\cdot\vec{p}}\, d\vec{p} \\ V(\vec{b},\omega,\vec{s}) &= e^{i\frac{\omega}{c}\vec{b}\cdot\vec{s}} \times \mathcal{F}(\vec{b},\omega) \end{aligned} \tag{1}$$

The Position of a point in the image plane, which is perpendicular to the direction on the source $\vec{s}$, is designated by a two-dimensional vector $\vec{p}$ which can be expanded at two orthogonal vectors $\vec{p}_x$, $\vec{p}_y$. The second ort, $\vec{p}_y$, is defined as a unit vector laid in the plane of source vector $\vec{s}$ and the celestial pole vector $\vec{z} = (0,0,1)^\top$. The first ort, $\vec{p}_x$, is perpendicular to both $\vec{s}$ and $\vec{p}_y$, so that $(\vec{p}_x, \vec{p}_y, \vec{s})$ forms the right triad. Vector $\vec{p}_x$ points towards the direction of decrease of right ascension, and $\vec{p}_y$ points towards the direction of increase of increase of declination.

$$\begin{aligned} \vec{p}_x &= \frac{\vec{s}\times\vec{z}}{|\vec{s}\times\vec{z}|} \\ \vec{p}_y &= \frac{\vec{s}\times\vec{p}_x}{|\vec{s}\times\vec{p}_x|} \end{aligned} \tag{2}$$

The proof of the van Cittert–Zernike theorem can be found in physics textbooks, for instance in Born & Wolf (2002). The amplitude of the coherence function, phase delay τ_p and group delay τ_g, also depends on the harmonic of the Fourier-transform of the source brightness distribution:

$$\begin{aligned} &\mathrm{Amp}(\vec{b},\omega,\vec{s}) = \sqrt{\mathrm{Re}^2(\mathcal{F}) + \mathrm{Im}^2(\mathcal{F})} \\ &\tau_p = \tfrac{1}{c}\vec{b}\cdot\vec{s} + \frac{1}{\omega}\mathrm{arctg}\frac{\mathrm{Im}(\mathcal{F})}{\mathrm{Re}(\mathcal{F})} + O(c^{-2}) \\ &\tau_g = \tfrac{1}{c}\vec{b}\cdot\vec{s} + \frac{\mathrm{Re}(\mathcal{F})\frac{\partial}{\partial\omega}\mathrm{Im}(\mathcal{F}) - \mathrm{Im}(\mathcal{F})\frac{\partial}{\partial\omega}\mathrm{Re}(\mathcal{F})}{\mathrm{Re}^2(\mathcal{F}) + \mathrm{Im}^2(\mathcal{F})} \\ &\qquad + O(c^{-2}) \end{aligned} \tag{3}$$

The second term in the expression for delays is zero if the source is point-like, and therefore, it describes the contribution of source structure.

The unmodeled source structure contribution causes both random and systematic errors in VLBI results, so it is desirable that this term should be accounted for in the reduction model. Although the amplitude of the coherence function is not used directly in geodetic VLBI data analysis, it is important to have a realistic prediction of this quantity during scheduling, in order to correctly calculate the integration time required for reaching a targeted signal-to-noise ratio.

It has been demonstrated many times since the 1980s, for instance, Cotton (1980); Zeppenfeld (1993); Sovers (2002), that information from source maps produced by the hybrid mapping algorithm can be applied for solving or at least alleviating the problem. However, using sources maps for scheduling and data reduction did not become a routine analysis procedure, because maps were not available for the majority of the sources. The situation has recently changed dramatically. Long-term projects of producing maps from the current and past VLBA and Australian LBA observations under the RDV, the VLBA Calibrator survey (VCS), and the southern survey projects yielded maps for almost all the sources ever observed under geodetic and astrometric programs. This paper is focused on using this information. In section 2, the image database is described. In section 3, the procedure for creation the new list of geodetic sources is outlined. in section 4, I discuss approaches for using source maps for scheduling. In section 5 problems of using maps for data reduction are mentioned.

2 Image database

Although astronomers have produced images from analysis of VLBI observations from early 1970s, to date there is no a central image repository. Pictures of contour maps of observed sources may be found in literature, however, using source structure information for scheduling and data reduction requires a representation of the two-dimensional function of the brightness distribution in a digital form, not in a form of nice pictures.

I created the image database using maps produced by Dr. Yu. Y. Kovalev, A. Pushkarev, A. Fey, G. Taylor, N. Corey, R. Ojha, members of the MOJAVE team and others who kindly agreed to make results of their work publicly available. These maps were made by analyzing VLBI observations in the framework of the RDV, VCS, MOJAVE, and VIPS projects observed at the VLBA. The database contains 1) images in fits-image format, 2) the visibility data calibrated using both the a priori antenna gains and system temperatures, as well as the a posteriori gain corrections determined by the hybrid image restoration algorithm, 3) auxiliary files.

The database consists of two levels. At the first level, the data are presented in the form at which the analyst has provided them. The data in the `image_orig` directory are split into 63 subdirectories which correspond either to a project or a project segment.

At the second level, the data are re-arranged to the form which is suitable to automatic processing. First, all sources are renamed to 10-character long IAU J2000-names. Second, all files related to a given source are put in the subdirectory which has the same name as the source. Third, the data files are renamed. The data file has name in the form: `SSSSSSSSSS_B_DDDDDDDDDD_AAA_TTT.EEEE`, where `SSSSSSSSSS` is the 10-character long IAU J2000 source name, `B` is the observing band: one of S for 2.2 GHz, C for 5.0 GHz, X for 8.6 GHz, U for 15.0 GHz, K for 22 GHz and Q for 43 GHz; `DDDDDDDDDD` is the nominal start date of the experiment; `AAA` is the analyst code; `TTT` is the data type; and `EEE` is the file extension, which reflects the data format.

There are 5 files for each image with the following combinations of the data type and data format: 1) `uvs.fits` — calibrated visibility data in FITS-format; 2) `map.fits` — an image in the FITS-format. This file keeps both the image in the form of the pixel two-dimensional array and in the form of a an expansion over a set of δ-functions or, using another language, the so-called CLEAN-components. 3) `rad.ps` — a plot in the postscript format of the dependence of the calibrated visibility function, averaged over time within a scan and over intermediate frequencies within a band, as a function of the length of the projected baseline to the plane normal to the source direction. 4) `map.ps` — a contour map in the postscript format of the image convolved with the dirty beam. 5) `cfd.tab` — a table in the ascii format of the correlated flux density estimates: a) the total flux density integrated over the map, b) the median value of the correlated flux density at baselines shorter than 900 km;

Table 1. Statistics of sources in the database per band

Band	# sources	# images
S	3319	7894
C	1119	1119
X	3243	7947
U	299	2072
K	270	890
Q	132	267

Table 2. The number of images at X and S band at each declination zone

Zone	total	X and S		X or S	
$\delta > -45^\circ$	3518	3044	86.5%	3336	94.8%
$\delta < -45^\circ$	143	4	2.7%	26	18.2%

c) the median value of the correlated flux density at baselines longer than 5000 km; d) the rms of the image noise.

Finally, the headers in files with visibilities and images in FITS-format were modified: the verbose history comments are removed and additional meta-information is included: a) precise source position and its errors; b) the Table of estimates of the correlated flux density; c) names of the authors who produced the image; d) the URL of the project; e) references to the papers related to the project.

To date, the database level 2 has 125,126 files of 20189 images of 3991 sources. For about 1/3 of these sources, 1440 objects, images at more than one epoch are available. Several experiments were processed by two independent analysts. Both versions of images are present in the database. The statistics of sources in the databases is presented in Table 1.

Since the vast majority of the maps were produced by analyzing observations at the VLBA, the distribution of sources with available images is quite different in the northern and southern hemispheres. The separate statistics are presented in Table 2. Among sources with declination $> -45^\circ$ that are not imaged, the majority of them are too weak and do not have enough data collected in order to produce a meaningful image.

The first[1] and the second[2] level of the image database is available in the Internet.

[1] `http://lacerta.gsfc.nasa.gov/image_orig/`
[2] `http://lacerta.gsfc.nasa.gov/vlbi/images/`

3 List of geodetic sources

The image database was used for selecting the list of sources best suitable for using in VLBI geodetic observing programs. Three criteria played a role in selection: 1) correlated flux density at long baselines; 2) compactness; 3) low spread with respect to a smooth line at plots of dependence of the correlated flux density on the length of the projected baseline. The rational for excluding weak sources is obvious: the formal uncertainties are reciprocal to the correlated flux density. The sources with extended structure, i.e. low compactness, are avoided, because the maps with high dynamic range are required for adequate modeling source structure effects. The sources with a highly asymmetric core that exhibit a significant spread at plots of dependence of the correlated flux density versus the length of the projected baseline were not selected because their images have a tendency to evolve to double and more complex structure, and remaining errors for correction for source structure using non-perfect maps may still be rather high.

The selection procedure consists of several steps. At the first step, the median correlated flux density at baselines with projected length longer than 5000 km were computed for all the sources using the calibrated visibility data. Then the ratio of the correlated flux density at long baselines to the correlated flux density integrated over the map, the so-called compactness index, was computed for each source. The closer the compactness index is to unity, the greater the share of radiation that comes from the unresolved detail of the source. Finally, the sources that have the median correlated flux density at long baselines > 200 mJy in the declination zone $[+10^\circ, +40^\circ]$ and > 300 mJy at other part of the sky were selected. If images at different epochs were available, the source was selected if it had the correlated flux density greater than the threshold for at least one epoch. In total, 584 objects were selected at the first step.

During the second step, images were scrutinized using a Web-oriented software, and for those objects that had maps from more than one epoch, a "representative image" was manually selected. By default, the last epoch is considered as representative. If the circumstances of observations were not favorable, and the *uv*-coverage was poor, another epoch with an image of better quality was selected using subjective criteria.

Figure 1. Example of the source map with the suitability class 1 ("perfect")

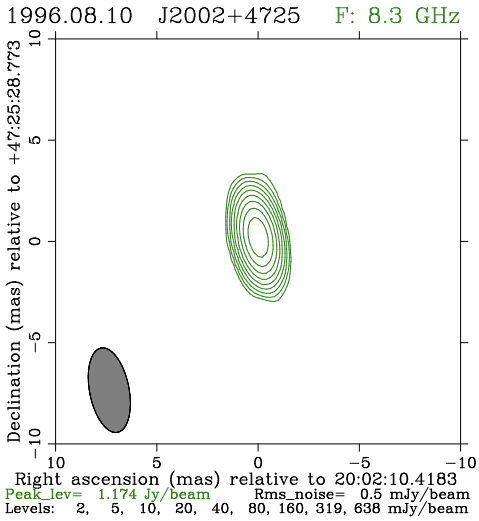

Figure 2. Example of the plot of dependence of the correlated flux density on the length of the projected baseline for a source with the suitability class 1 ("perfect")

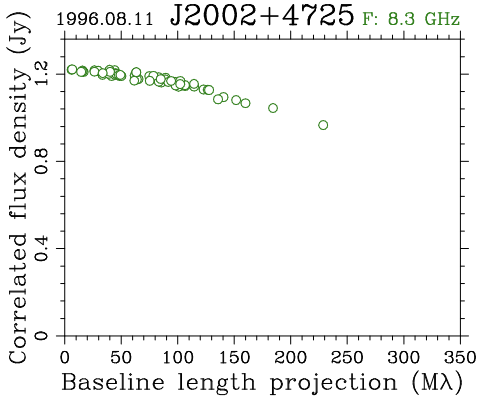

During the third step, a class in the range of 1–4 as a measure of suitability for geodetic observations was assigned to each source.

- Suitability class 1 ("perfect") means that at both bands the source has a compactness index greater than 0.8, and it has a very small spread at plots of calibrated visibilities versus the length of the baseline projected to the plane normal to the source direction, because it does not have image asymmetries (Figures 1–2).

- Suitability class 2 ("good") means that at both bands the source has a compactness index in the range of 0.4–0.8, the scatter of the calibrated visibilities versus the length of the projected baseline about the best fit smooth line is less than 20%, the image does not show significant extended details, and the source core does not have significant deviations from the elliptical structure.

- Suitability class 3 ("bad") means that the source is still detected even at long baselines at both bands, but either has a compactness index is less than 0.4 or has significant image asymmetries that cause a large spread at plots of calibrated visibilities versus the length of the baseline projected to the plane normal to the source direction. (Figures 3–4).

Figure 3. Example of the source map with the suitability class 3 ("bad")

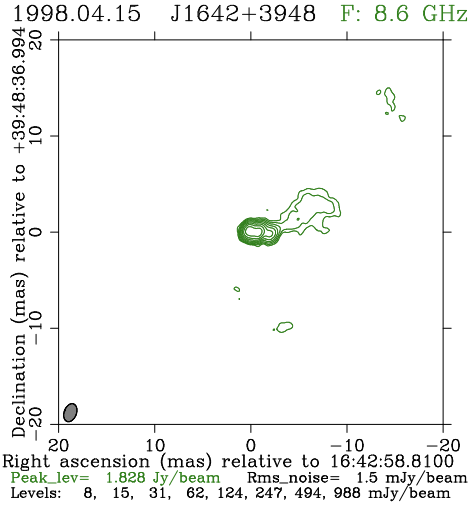

Figure 4. Example of the plot of dependence of the correlated flux density on the length of the projected baseline for a source with suitability class 3 ("bad")

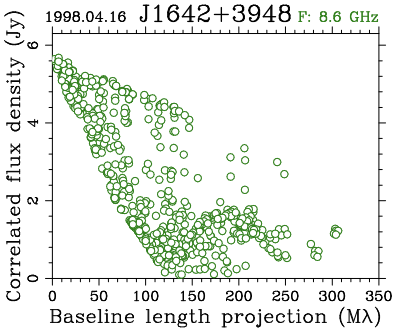

- Suitability class 4 ("unsuitable") means that at least at one band the source is too weak and not compact enough to be even detected

Table 3. The distribution of sources over classes at the old, pre–2007 list and proposed, post–2007 list

Class	pre–2007 list	post–2007 list
1	**4**	**45**
2	**43**	**185**
3	50	0
4	14	0
total	117	230

at baselines longer than 5000 km, i.e. the correlated flux density at long baselines is less than 100 mJy.

The initial classes were assigned automatically, and they were adjusted manually with use of a Web-oriented software. The sources with class 1 and 2, in total 230 objects, are recommended for observing in geodetic programs. The new list is available on the Web[3]. In comparison with the old, pre–2007 list, the total number of sources in the proposed geodetic list is doubled, but many strong asymmetric sources were removed. Approximately 40% of the sources from the old list were retained. Table 3 summarizes the sources distribution over classes.

4 Using maps for scheduling

The preferable way for using source structure information for scheduling is to use images in the form of an expansion over a set of δ-functions. This work is in progress. As an intermediate step, a simplified model of source structure was implemented in the scheduling software SKED. The dependence of the correlated flux density on the length of the projected baseline was approximated by a polynomial of the 3-rd degree using the least squares. These polynomials were used for computing the table of dependence of the correlated flux density on the length of the projected baseline with a step of 1000 km. Since the selection criteria for the proposed list of geodetic sources were developed to avoid sources with a significant spread of visibilities with respect to a smooth line, this simplified approach is expected to have an error of no more than 20–30% for these sources. Precise prediction of the fringe amplitude allows us to reduce the rate of non-detections and further optimize the schedule.

[3] http://vlbi.gsfc.nasa.gov/pet/discussion/sou_list

5 Using maps for data reduction

Computation of the contribution of source structure to group delay according to equation 3 is straightforward (Charlot (1990)), provided the two-dimensional Fourier-transform of the image is given. However, the true image of the source is not known, only its approximate model. The hybrid CLEAN method, traditionally used for image restoration in analysis of VLBI data, represents the brightness distribution in the form of the expansion over a set of δ-functions:

$$I(p_x, p_y) = \sum_i^n A_i \, \delta(x - p_{xi}, y - p_{yi}) \qquad (4)$$

The Fourier-transform of the brightness distribution in this form is a sum of sinusoids which fits the visibility data at points of observation. It should be noted that the representation of an image of an active galactic nuclei object in the form of a set of δ-functions is at odds with physical models of these sources that require a certain degree of smoothness in the brightness distribution. Smooth, good-looking images presented in figures 3 and 1 are produced by convolving $I(p_x, p_y)$ with the so-called "clean beam" in the form of a Gaussian function that represents an idealized response of the array with no gaps in the uv-coverage. However, this smoothed image does not fit the visibility data.We need to use images produced in one experiment for calibrating another observing session. The contribution of source structure to group delay is computed at the points at the uv-plane that do not corresponds to the points of visibilities used for producing maps. In fact, maps are used for extrapolation of the phase and amplitude of visibility data. Thus, the mathematical model of the source brightness distribution should correctly represent not only the visibility data at the points at the uv-plane where observations were made, but serve as an adequate approximation of the complex interferometric coherence function at the entire uv-plane. This discussion illustrates the difficulties in using source maps for astronomical reductions.

I attempted to apply group delay source structure contribution to VLBI data. The source brightness distribution was presented in the form of an expansion over a set of δ-functions. The contribution to group delay was computed this way:

$$
\begin{aligned}
B_i &= \vec{b}\,\vec{p_x} p_{xi} + \vec{b}\,\vec{p_x} p_{yi} \\
R &= \sum_i^n A_i \cos\left(\frac{\omega}{c} B_i\right) \\
I &= \sum_i^n A_i \sin\left(\frac{\omega}{c} B_i\right) \\
R' &= -\sum_i^n A_i \frac{B_i}{c} \sin\left(\frac{\omega}{c} B_i\right) \\
I' &= \sum_i^n A_i \frac{B_i}{c} \cos\left(\frac{\omega}{c} B_i\right) \\
\tau_{gr} &= \frac{R\,I' - I\,R'}{R^2 + I^2}
\end{aligned}
\tag{5}
$$

The dependence of brightness distribution on frequency within the observed band was ignored.

I used a short dataset of 89,628 observations of the CONT05 campaign collected at the 11-station network for 15 consecutive days starting from 2005.09.12.

First, I ran the reference solution. Positions of all stations, coordinates of all sources, as well as clock function, atmospheric zenith path delay and troposphere gradients modeled by a linear spline were estimated. No-net-rotation constraints were applied on estimates of site positions and source coordinates. The rms of post-fit residuals for the reference solution was 13.947 ps.

I computed The source structure contribution for X and S bands for each source in that campaign using expression 5 and applied it to data reduction.

Surprisingly, the rms of post-fit residuals increased to 14.204 ps. In order to investigate the problem, I tried an alternative approach. The source structure was not applied to data reduction, but was used as a partial derivative for estimation of the admittance factor, common for all sources. If the model source structure signal is not present in the data the admittance is close to zero. If the model of source structure is perfect, the estimate of the admittance will be close to 1. The estimate was 0.409 ± 0.003 and the rms of post-fit residuals dropped to 13.698 ps. Further analysis showed that the map noise with low spatial frequencies spread over the image and leaks as a noise in group delays with high frequencies in time delay (refer to figure 5). The noise is significantly enhanced for group delay contribution because that contribution depends on the partial derivative of noisy data. Apparently, the high frequency contribution to group delay is an artifact of image restoration.

Figure 5. The contribution to group delay from very compact source J1018+0530 computed using the raw image.

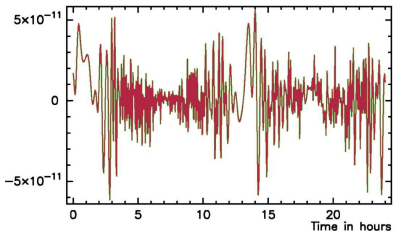

I ran another solution, for which I discarded the components of the image with amplitude less than 2σ of image noise. The admittance factor estimate was 0.482 ± 0.004 and the rms of post-fit residuals was 13.691 ps.

Another way to suppress high frequency noise in structure group delay contribution is to apply a digital diaphragm. I multiplied the image by the circular Gaussian function centered at the phase center of the image with the FWHM 10 mas at X-band and 40 mas at S-band. The admittance factor estimate was 0.652 ± 0.005 and the rms of post-fit residuals was 13.627 ps. Finally, the solution with applied source structure contribution to group delay computed using the map with digital diaphragm applied gave the rms of post-fit residuals 13.716 ps, less than the rms of the reference solution.

A more thorough study of the optimal strategy for computing the contribution of source structure to group delay is necessary.

References

Born, M., E. Wolf, Principles of optics, 1980, Pergamon Press.

Charlot, P., Astron. J., 1990, 99., 1309.

Charlot, P., in IVS General meeting proceedings, 2002, 233.

Cotton, W. D., in Radio interferometry technique for geodesy., p. 193, 1980

Sovers, O.J., P. Charlot, A. Fey, D. Gordon, in IVS General meeting proceedings, 2002, 243.

Zeppenfeld, G. "Einflüsse der Qullenstruktur in der Praxis der geodatischen VLBI, N 80, Mittailungen aus den Geodätischen Instituten der Universität Bonn, 1993.